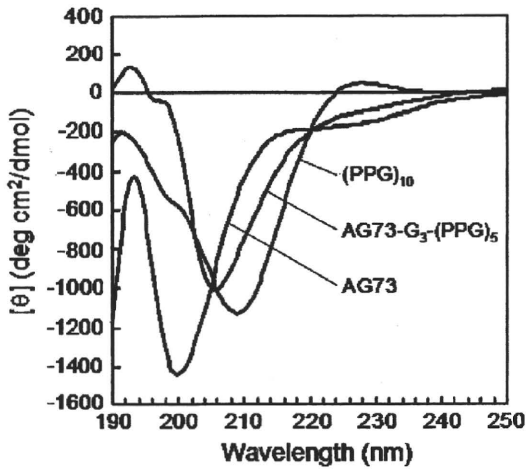

Fig. 1. Circular dichroism spectra of $(PPG)_{10}$, AG73 and AG73-G_3-$(PPG)_5$ in water.

point at 220 nm. The results suggest that the CLP region of AG73-G_3-$(PPG)_5$ also forms the PP-II structure. It is well known that the PP-II structure is the predominant secondary structure in collagen triple-helix. In addition, the PP-II structure of $(PPG)_n$ repetitive sequence exposes hydrophobic five-membered rings of Pro residues. Therefore, it is inferred that $(PPG)_n$ is adsorbed onto PLA films via hydrophobic interaction.

3.2. Surface characterization of peptide-adsorbed PLA films

To compare the hydrophilicity of the peptide-adsorbed PLA film surfaces, the water contact angle was measured (Table 1). The water contact angle of non-adsorbed PLA films was 79.1 ± 1.2°, which indicates a hydrophobic surface. After adsorption of $(PPG)_{10}$, AG73 and AG73-G_3-$(PPG)_5$, the water contact angle changed to 70.1 ± 3.9°, 31.2 ± 2.1° and 55.6 ± 1.9°, respectively. The water contact angle drastically decreased with AG73 and AG73-G_3-$(PPG)_5$ adsorption, but with $(PPG)_{10}$ adsorption the decrease was considerably less. It seems that the surface wettability of peptide-adsorbed PLA films corresponded to the hydrophilicity of the peptides, i.e. $(PPG)_{10}$ is more hydrophobic than AG73 and AG73-G_3-$(PPG)_5$. Safinia et al. reported that the PLA film surface shows a negative ζ-potential at physiological pH [32] because of a carboxyl group at the terminal of the PLA molecule. Therefore, the results suggest that these peptides are adsorbed onto PLA film via hydrophobic or electrostatic interactions.

The XPS N1s spectrum is shown in Fig. 2. The XPS spectra of $(PPG)_{10}$-, AG73- and AG73-G_3-$(PPG)_5$-adsorbed PLA films exhibited a N1s peak corresponding to amino acids. In order to compare the adsorbed peptide ratio on PLA films, the elemental ratios are summarized in Table 2. N1s was not detected clearly because PLA itself does not contain nitrogen. The N1s/C1s ratios were 0.07, 0.09 and 0.18, and the N1s/O1s ratios were 0.03, 0.04 and 0.09. The N1s/C1s and N1s/O1s ratios were increased with peptide adsorption; in particular, the highest values were shown for AG73-G_3-$(PPG)_5$. The AG73-G_3-$(PPG)_5$ might be adsorbed at high density via hydrophobic interaction between $(PPG)_5$ region and PLA. The reason for the decrease in water contact angle of AG73-G_3-$(PPG)_5$-adsorbed PLA film (Table 1) is that the hydrophilic AG73 region in AG73-G_3-$(PPG)_5$ was partially exposed to solution. Ji et al. also indicated that the poly(ethylene oxide–propylene oxide–ethylene oxide) amphiphilic triblock copolymer bearing RGD tripeptides adsorbed onto PLA films through hydrophobic interaction, and its hydrophilic regions were exposed to solution phase [11]. As a result, the AG73-G_3-$(PPG)_5$ adsorbs via hydrophobic interaction and constructs an ECM-like layer on the PLA film surface.

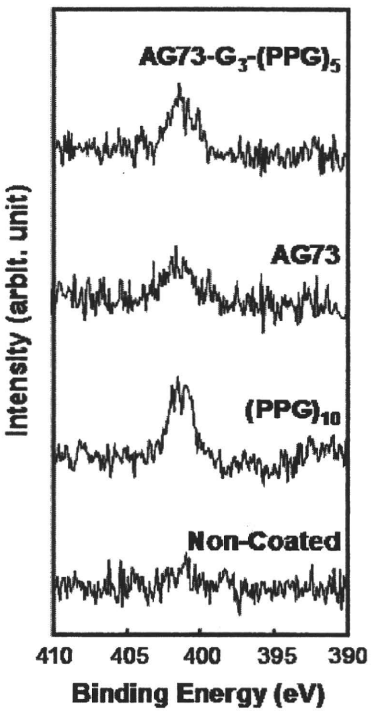

Fig. 2. XPS spectra of the N1s region of peptide-adsorbed PLA films.

Table 1
Water contact angle of peptide-adsorbed PLA films.

	CA (°)
Non-adsorbed	79.1 ± 1.2
$(PPG)_{10}$	70.1 ± 3.9
AG73	31.2 ± 2.1
AG73-G_3-$(PPG)_5$	55.6 ± 1.9

Table 2
Elemental ratio of nitrogen to carbon (N1s/C1s) or oxygen (N1s/O1s) measured by XPS.

	PLA	$(PPG)_{10}$	AG73	AG73-G_3-$(PPG)_5$
N1s/C1s	0.01	0.07	0.09	0.18
N1s/O1s	0.00	0.03	0.04	0.09

3.3. Neurite outgrowth activity of peptide-adsorbed PLA films

The morphology of PC12 cells on peptide-adsorbed PLA films is shown in Fig. 3a, and the number of adhered PC12 cells with or without neurites is summarized in Fig. 3b. On the naked and $(PPG)_{10}$-adsorbed PLA films, PC12 cells (~230 cells mm^{-2}) did not adhere well enough, and so neurite outgrowth could not be found. This indicates that $(PPG)_n$ itself does not support bioactivity for cell adhesion or neurite outgrowth. Meanwhile, on AG73- and AG73-G_3-$(PPG)_5$-adsorbed PLA films, the adhesion of PC12 cells was improved to more than 300 cells mm^{-2}. Neurite outgrowth also occurred, i.e. the number of PC12 cells with neurites was more than 75% on both AG73- and AG73-G_3-$(PPG)_5$-adsorbed PLA films. In contrast, the mechanisms of adsorption of these films must be different from each other since the physicochemical properties of AG73 and AG73-G_3-$(PPG)_5$ are quite dissimilar. As mentioned above, they are considered to be adsorbed onto PLA films via

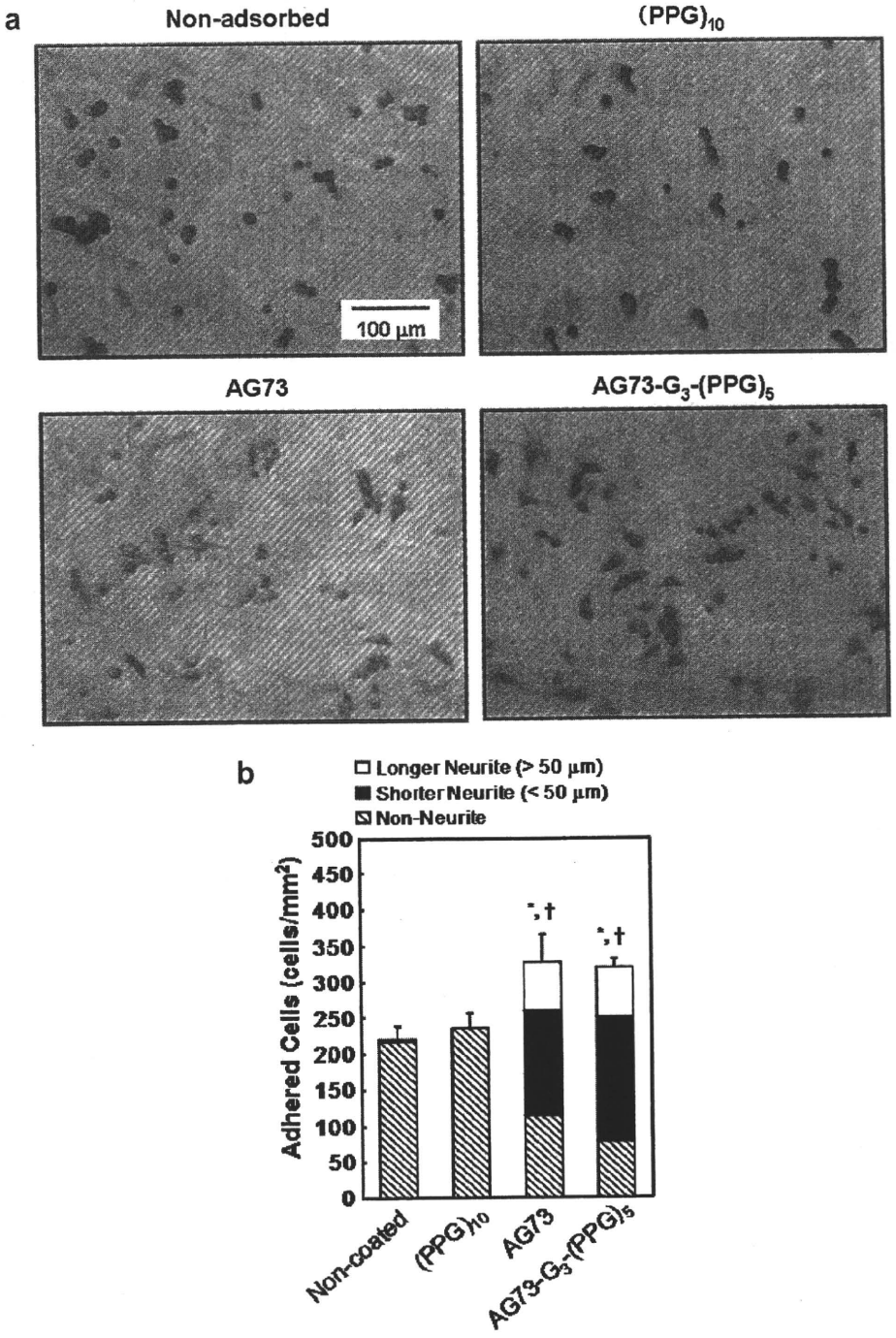

Fig. 3. Neurite outgrowth activity of PC12 cells on peptide-adsorbed PLA films. (a) Morphology of PC12 cells on peptide-adsorbed PLA films after 24 h. (b) The number of adhered PC12 cells on peptide-adsorbed PLA films with and without neurites. $^{*}P < 0.05$ when AG73 and AG73-G_3-$(PPG)_5$ groups compared with non-coated group; $^{\dagger}P < 0.05$ when AG73 and AG73-G_3-$(PPG)_5$ groups compared with $(PPG)_{10}$ group.

electrostatic and hydrophobic interactions, respectively. It is anticipated that under physiological conditions, adsorption of AG73-G_3-$(PPG)_5$ is more stable than that of AG73.

In order to evaluate the stability of the adsorbed AG73-G_3-$(PPG)_5$, neurite outgrowth assay was performed on AG73- and AG73-G_3-$(PPG)_5$-adsorbed PLA films after washing with 1.0 M NaCl aqueous solution (Fig. 4). In the case of AG73-adsorbed PLA films, the number of adhered PC12 cells is decreased to below 60% by 1.0 M NaCl washing, but the ratio of PC12 cells with neurites remains unchanged. After 1.0 M NaCl washing, the water contact angles of $(PPG)_{10}$-, AG73- and AG73-G_3-$(PPG)_5$-adsorbed PLA films changed from $70.1 \pm 3.9°$, $31.2 \pm 2.1°$ and $55.6 \pm 1.9°$ to $70.3 \pm 1.5°$, $60.0 \pm 1.3°$ and $54.6 \pm 4.2°$, respectively. That is, the water contact angle of the AG73-adsorbed PLA films was drastically increased by 1.0 M NaCl washing, but that of AG73-G_3-$(PPG)_5$-adsorbed films was changed a little. These results indicated that adsorbed AG73 seemed to be partially removed by 1.0 M NaCl washing, and the remaining AG73 expressed neurite outgrowth-promoting activity, because AG73 was mainly adsorbed via electrostatic interaction. Meanwhile, the number of adhered PC12 cells was not changed and neurite outgrowth was also found on AG73-G_3-$(PPG)_5$-adsorbed PLA films after washing with H_2O or 1.0 M

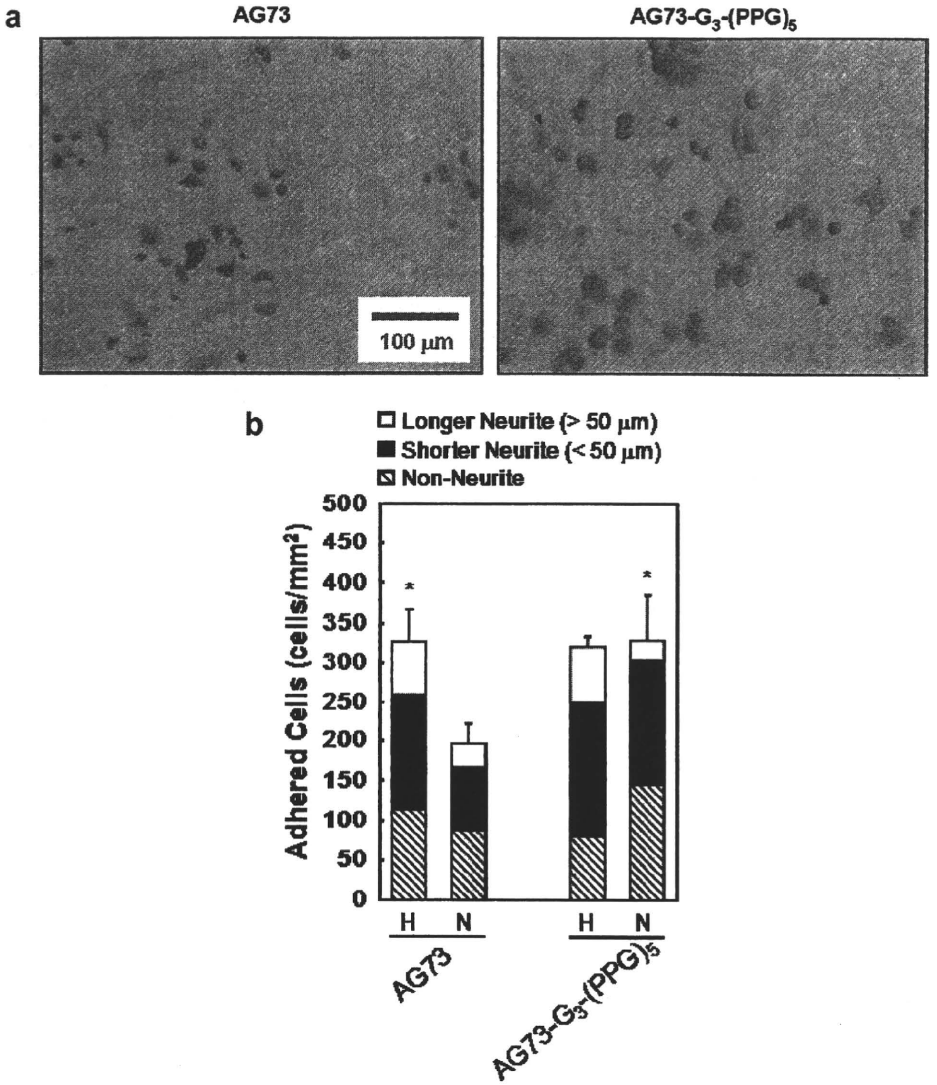

Fig. 4. Neurite outgrowth activity of PC12 cells on AG73- and AG73-G_3-$(PPG)_5$-adsorbed PLA films after washing with H_2O (H) or 1.0 M NaCl aq. (N). (a) Morphology of PC12 cells after 24 h. PLA films were modified with peptides, washed with 1.0 M NaCl and subjected to PC12 cell culture. (b) The number of adhered PC12 cells on peptide adsorbed PLA films with and without neurites. * $P < 0.05$ when AG73 (H) and AG73-G_3-$(PPG)_5$ (N) groups are compared with AG73 (N) group.

NaCl. Hydrophobic interaction generally becomes stronger in the presence of salts because of the dehydration of the surface and adsorbents. The ratio of PC12 cells with neurites was slightly decreased by 1.0 M NaCl washing, because a partial AG73-G_3-$(PPG)_5$ was adsorbed by PLA films via electrostatic interaction. As result, it is proposed that PLA films adsorb AG73-G_3-$(PPG)_5$ mainly by hydrophobic interaction, and an ECM-like layer composed of structural protein and biosignalling sequences is formed. It is known that animal-derived collagen, like laminin, also promotes neurite outgrowth, because it is a fusion protein that combines a structural protein with many biosignal sequences [33]. Neurite outgrowth is mainly promoted by biosignal sequences in collagen, and it must be supported by the structural properties of these sequences. We believe that the structural properties of the ECM-like layer composed of AG73-G_3-$(PPG)_5$ creates a synergy with AG73 biosignalling for promoting neurite outgrowth.

4. Conclusion

Hydrophobic peptide-based interfacial adsorption onto PLA films and film stability have been characterized. Collagen-laminin mimics peptide AG73-G_3-$(PPG)_5$ and forms the hydrophobic PP-II structure in the $(PPG)_5$ region. Therefore, AG73-G_3-$(PPG)_5$ was capable of exhibiting stable adsorption onto PLA films via hydrophobic interaction, resulting in promotion of neurite outgrowth of PC12 cells. Furthermore, AG73-G_3-$(PPG)_5$, which is composed of biosignalling and structural protein-like sequences, forms an ECM-like layer on PLA films. It has recently been noted that the mechanical and morphological properties of ECMs are important for controlling stem cell differentiation [34]. The hydrophobic adsorption of collagen-like peptide is expected to serve as a surface modification technique of PLA films for controlling the biological properties of cells.

Acknowledgements

The authors thank Dr. Aasako Yamayoshi and Prof. Akira Murakami at the Kyoto Institute of Technology for assistance with the circular dichroism measurements. This work was partly supported by a Grant-in-Aid for Scientific Research (KAKENHI) promoted by the Ministry of Education, Culture, Sports and Technology, Japan.

Appendix A. Figures with essential color discrimination

Certain figures in this article, particularly Figs. 3 and 4, are difficult to interpret in black and white. The full color images can be found in the on-line version, at doi: 10.1016/j.actbio.2009.12.001.

References

[1] Lanza R, Langer R, Vacanti J, editors. Principles of tissue engineering. Amsterdam and Boston, MA: Elsevier/Academic Press; 2007.
[2] Tabata Y. Biomaterial technology for tissue engineering applications. J R Soc Interface 2009;6:S311–24.
[3] Ma Z, Mao Z, Gao C. Surface modification and property analysis of biomedical polymers used for tissue engineering. Colloids Surf B Biointerfaces 2007;60:137–57.
[4] Gupta B, Revagade N, Hilborn J. Poly(lactic acid) fiber: an overview. Prog Polym Sci 2007;32:455–82.
[5] Jiao YP, Cui FZ. Surface modification of polyester biomaterials for tissue engineering. Biomed Mater 2007;2:R24–37.
[6] Khorasani MT, Mirzadeh H, Irani S. Plasma surface modification of poly(L-lactic acid) and poly(lactic-co-glycolic acid) films for improvement of nerve cells adhesion. Rad Phys Chem 2008;77:280–7.
[7] Ma Z, Gao C, Ji J, Shen J. Protein immobilization on the surface of poly-L-lactic acid films for improvement of cellular interactions. Eur Polym J 2002;38:2279–84.
[8] Yamaoka T, Hotta Y, Kobayashi K, Kimura Y. Synthesis and properties of malic acid-containing functional polymers. Int J Biol Macromol 1999;25:265–71.
[9] Yamaoka T, Takebe Y, Kimura Y. Surface modification of poly(L-lactic acid) film with bioactive materials by a novel direct alkaline treatment process. Kobunshi Ronbunshu 1998;55:328–33.
[10] Zhu H, Ji J, Barbosa MA, Shen J. Protein electrostatic self-assembly on poly(DL-lactide) scaffold to promote osteoblast growth. J Biomed Mater Res B Appl Biomater 2004;71:159–65.
[11] Ji J, Zhu H, Shen J. Surface tailoring of poy(DL-lactic acid) by ligand-tethered amphiphilic polymer for promoting chondrocyte attachment and growth. Biomaterials 2004;25:1859–67.
[12] Matsuno H, Sekine J, Yajima H, Serizawa T. Biological selection of peptides for poly(L-lactide) substrates. Langmuir 2008;24:6399–403.
[13] Oh SH, Kim JH, Song KS, Jeon BH, Yoon JH, Seo TB, et al. Peripheral nerve regeneration within an asymmetrically porous PLGA/Pluronic F127 nerve guide conduit. Biomaterials 2008;29:1601–9.
[14] Weeks BS, Nomizu M, Ramachandran RS, Yamada Y, Kleinman HK. Laminin-1 and the RKRLQVQLSIRT laminin-1 α1 globular domain peptide stimulate matrix metalloproteinase secretion by PC12 cells. Exp Cell Res 1998;243:375–82.
[15] Koide T. Designed triple-helical peptides as tools for collagen biochemistry and matrix engineering. Philos Trans R Soc B 2007;362:1281–91.
[16] Abraham LC, Zuena E, Perez-Ramirez B, Kaplan DL. Guide to collagen characterization for biomaterial studies. J Biomed Mater Res B Appl Biomater 2008;87:264–85.
[17] Jenkins CL, Raines RT. Insights on the conformational stability of collagen. Nat Prod Rep 2002;19:49–59.
[18] Engel J, Bachinger HP. Structure, stability and folding of the collagen triple helix. Top Curr Chem 2005;247:7–33.
[19] Okuyama K. Revisiting the molecular structure of collagen. Connect Tissue Res 2008;49:299–310.
[20] Kakinoki S, Hirano Y, Oka M. On the stability of polyproline-I and II structures of proline oligopeptides. Polym Bull 2005;53:109–15.
[21] Kobayashi Y, Sakai R, Kaniuchi K, Isemura T. Physicochemical analysis of (Pro-Pro-Gly)$_n$ with defined molecular weight-temperature dependence of molecular weight in aqueous solution. Biopolymers 1970;9:415–25.
[22] Gough CA, Anderson RW, Bhatnagar RS. The role of bound water in the stability of the triple-helical conformation of (Pro-Pro-Gly)$_{10}$. J Biomol Struct Dyn 1998;15:1029–37.
[23] Stetefeld J, Frank S, Jenny M, Schulthess T, Kammerer RA, Boudko S, et al. Collagen stabilization at atomic level: crystal structure of designed (GlyProPro)$_{10}$ folden. Structure 2003;11:339–46.
[24] Inada Y, Morimoto S, Moroi K, Endo K, Nakamura T. Surgical relief of causalgia with an artificial nerve guide tube: successful surgical treatment of causalgia (Complex Regional Pain Syndrome Type II) by in situ tissue engineering with a polyglicolic acid-collagen tube. Pain 2005;117:251–8.
[25] Andair-Kirk TL, Senior RM. Fragments of extracellular matrix as a mediators of inflammation. Int J Biochem Cell Biol 2008;40:1101–10.
[26] Greene LA, Tischler AS. Establishment of a noradrenergic clonal line of rat adrenal pheochromocytoma cells which respond to nerve growth factor. Proc Natl Acad Sci USA 1976;73:2424–8.
[27] Mochizuki M, Kadoya Y, Wakabayashi Y, Kato K, Okazaki I, Yamada M, et al. Laminin-1 peptide-conjugated chitosan membranes as a novel approach for cell engineering. FASEB J 2003;17:875–7.
[28] Ichikawa N, Kasai S, Suzuki N, Nishi N, Oishi S, Fujii N, et al. Identification of neurite outgrowth active sites on the laminin α4 chain G domain. Biochemistry 2005;44:5755–62.
[29] Collins TJ. ImageJ for microscopy. Biotechniques 2007;43:S25–30.
[30] Jenness DD, Sprecher C, Curtis J. Circular dichroism of collagen, gelatin, and poly(proline) II in the vacuum ultraviolet. Biopolymers 1976;15:513–21.
[31] Khew ST, Tong YW. Characterization of triple-helical conformations and melting analyses of synthetic collagen-like peptides by reversed-phase HPLC. J Chromatogr B Analyt Technol Biomed Life Sci 2007;858:79–90.
[32] Safinia L, Datan N, Höhse M, Mantalaris A, Bismarck A. Towards a methodology for the effective surface modification of porous polymer scaffolds. Biomaterials 2005;26:7537–47.
[33] David CT, Leonard AF, Salvatore C. Identification of a cell-surface protein involved in PC12 cell-substratum adhesion and neurite outgrowth on laminin and collagen. J Neurosci 1989;9:3287–96.
[34] Hwang NS, Varghese S, Elisseeff J. Controlled differentiation of stem cells. Adv Drug Deliv Rev 2008;60:199–214.

///VSP///

Journal of Biomaterials Science 22 (2011) 627–640

Journal of **BIOMATERIALS SCIENCE**
brill.nl/jbs

Peripheral Nerve Regeneration and Electrophysiological Recovery with CIP-Treated Allogeneic Acellular Nerves

T. Ehashi [a], A. Nishigaito [a,b], T. Fujisato [a,c], Y. Moritan [b] and T. Yamaoka [a,*]

[a] Department of Biomedical Engineering, National Cardiovascular Center Research Institute, 5-7-1 Fujishiro-dai, Suita, Osaka 565-8565, Japan

[b] Department of Medical Engineering, Suzuka University of Medical Science, Suzuka, Japan

[c] Department of Biomedical Engineering, Osaka Institute of Technology, Osaka, Japan

Received 30 October 2009; accepted 19 January 2010

Abstract

Acellular nerve grafts are a desirable alternative to autografts, both because the source of acellular nerves is potentially unlimited and because they have the same matrix structure as natural nerves, which would facilitate axon growth from the defective nerve stump. Although some acellular nerves have been developed, most of them were studied in isogenic transplantation models and evaluated only by histological observation. In the present study, novel allogeneic acellular nerves prepared using the cold isostatic pressuring (CIP) method were developed and assessed as a potential substitute for autografts. The host immune response to acellular nerves and fresh nerves was analyzed using Lewis rats as donors and SD rats as recipients, which is the allogeneic transplantation model, by subcutaneous implantation for one month. In addition, sciatic nerve transplantation into a 10-mm nerve gap was carried out using the same model, and the axonal growth in acellular nerve transplantation was evaluated histologically and electrophysiologically, and compared with that of axons in the autograft transplant area. The subcutaneously implanted acellular nerves contained more macrophages and less vasculature than the allogeneic fresh nerves. In spite of these results of the subcutaneous implantation, Schwann cell infiltration in the graft transplanted into the sciatic nerve gap was observed after the short-term transplantation. The myogenic potential, which was measured as an index of electrophysiological function in acellular nerve transplantation, was also recovered in the long-term transplantation. Our results indicate that the acellular nerves developed herein have the potential to support nerve regeneration and might be useful as an alternative to autografts.

Keywords

Acellular nerve, allogeneic, electrophysiological study, cold isostatic pressuring treatment

* To whom correspondence should be addressed. Tel.: (81-6) 6833-5012; Fax: (81-6) 6835-5476; e-mail: yamtet@ri.ncvc.go.jp

DOI:10.1163/092050610X488250

1. Introduction

Autologous fresh nerves are commonly used in clinical applications for treating peripheral nerve defects. However, an alternative to the autologous nerves is needed because these nerves are available only in limited quantities, and also because their use causes concurrent healthy nerve dysfunction [1, 2]. In general, tissue-derived nerves are always preferable, since they possess a natural internal structure of extracellular matrix components, which can lead to cellular migration and nerve fiber elongation [3–7].

Cadaveric donor grafts are an attractive alternative to autologous nerves, and their supply is potentially unlimited. In 2001, clinical trials for cold-preserved nerve allografts were reported to cause severe peripheral nerve defects [8]. In that report, 6 patients exhibited successful nerve reconstruction by cadaveric nerve allograft transplantation. However, long-term systematic administration of immunosuppressant was required, and even with that degree of treatment, one of the patients still experienced immune rejection. Moreover, it has been reported that the rate of nerve regeneration using cold preserved allogeneic nerves is lower than that using autologous fresh nerves with immunosuppressant treatment [9].

For treatment without an immunosuppressant, various strategies to eliminate the immunogenicity of allogeneic nerves have been explored in different animal models, but the grafts revealed very poor completeness in comparison to that of the autografts [10–12]. The main strategies for reducing the immunogenecity of allografts or xenografts are thermal and chemical pretreatments of nerves [8, 13, 14]. These pretreatments can destroy or remove the donor cells, but the natural internal structure of the nerve tissue remains unchanged.

The thermal process involves repeated cycles of freezing and thawing of donor nerves. This process destroys the allogeneic antigen and eliminates allogeneic cells, and has been reported to decrease the host antigeneic response in some studies [8, 15]. However, the axonal growth in these grafts is slower than it is in fresh autografts or isogeneic grafts, because of the residual allogeneic cells in the graft [13]. The cellular debris in the graft leads to macrophage invasion and basal laminae damage, which delay the nerve regeneration [16–19].

Chemical processes to remove the donor cells with detergents have been studied not only for peripheral nerve tissue [14, 20, 21] but also for cardiac muscle [22], heart valves [23] and pericardium [24]. This process is more effective in removing the donor cells. However, it also causes more damage to the extracellular matrices than thermal pretreatment does [7, 25, 26]. In addition, it is difficult to completely remove the detergent from the graft, and the residual chemicals suppress tissue regeneration. Starting in 2002, decellularized human nerves which are processed with a combination of detergent decellularization, chondroitinase degradation and gamma-irradiation sterilization have been marketed by AxoGen in the USA. The decellularized nerve grafts are superior to the commercially available conduits but not as effective as isografts [27].

We have established a novel decellularization method using a cold isostatic pressuring (CIP) treatment [28]. This method has succeeded in removing the cellular components from pig blood vessels, heart valves and trachea. We have also reported on the excellent reconstruction of endothelial cells, fibroblasts and smooth muscle cells in acellular vessels 12 weeks after the transplantation [28]. Thus, novel allogeneic acellular nerve grafts that possess natural extracellular matrices were prepared by the CIP method and examined in this study. In fact, many studies have been performed to develop novel treatments as an alternative to autografts, and most of the acellular tissue transplantations have been studied using isogeneic transplantation models [2, 20, 29, 30]. However, only a few studies have focused on allogeneic transplantation [8, 21, 26, 31]. Moreover, the regeneration of nerves by pretreated nerve transplantation should be assessed functionally in addition to histological assessment. For example, there have been only a few studies focused on the conduction velocity [20, 32] or myogenic potential [20, 31] of the acellular nerve transplantation. Therefore, for this study, allogeneic acellular nerves were prepared from Lewis rat sciatic nerves, and transplanted into a sciatic nerve gap in SD rats. As a preliminary study, a 10-mm gap of sciatic nerve which is repaired by any other nerve graft substitute, was bridged with our acellular nerve grafts to evaluate their potential in nerve regeneration, and the axonal growth in the allogeneic acellular nerves was evaluated histologically and electrophysiologically.

2. Materials and Methods

2.1. Preparation of Acellular Nerves

All animal studies were performed in accordance with the guidelines of the Ministry of Health, Labour and Welfare of Japan, as well as the guidelines of our institution, and approved by the Institutional Animal Care and Use Committee at the National Cardiovascular Center Research Institute.

Approximately 30-mm lengths of the sciatic nerves were harvested from a male Lewis rat weighing 300–350 g (Japan SLC) and, after trimming their peripheral fat and connective tissues, the nerves were packed in a polyethylene pouch with Ca^{2+}-, Mg^{2+}-free phosphate-buffered saline (PBS; Invitrogen) and the air was expelled. The nerves were then treated with ultra high pressure of 980 MPa at 30°C for 10 min using a Dr. Chef high pressure food processor (Kobe Steel) to disrupt all cells, microorganisms and viruses inside the tissues. The cell debris was washed away by immersing the cells in endothelial cell growth medium (EGM-2 Bulletkit; Lonza) for 2 weeks at 37°C. Then, ethanol/PBS (80:20, v/v) was used to remove phospholipids, which lead to calcification of implants, and was removed by rinsing with PBS for 3 days.

The acellular nerves were morphologically and histologically compared with the untreated nerves. The decellularization efficiency and extra-cellular component morphology were evaluated by hematoxylin and eosin staining (HE staining). Briefly, the samples were fixed with 10% neutralized formalin, then dehydrated and

embedded in paraffin, sectioned at 8–10 μm, and captured on slide glasses. The slide glasses were immersed into Mayer's hematoxylin solution (Wako), rinsed with tap water, and counterstained with eosin solution (Wako).

2.2. *Subcutaneous Implantation*

The host body reaction to the allogeneic fresh nerves and allogeneic acellular nerves was investigated by subcutaneous implantation into rats. As the allogeneic transplantation model, we used Lewis rats and SD rats as donor and recipient animals, as described by Hudson *et al.* [17]. Three 13-week-old male SD rats (Japan SLC) were anesthetized with isoflurane inhalation. Two incisions were made in the dorsal skin on the back of each of three SD rats, and fresh or acellular nerves of a Lewis rat (10 mm long) were inserted into both subcutaneous spaces. Thus, one fresh nerve sample and one acellular nerve sample was implanted into the back of each of the three rats. After 4 weeks of implantation, all rats were killed humanely and the grafts were resected with the surrounding skin.

Angiogenesis and macrophage infiltration against the grafts was evaluated by HE staining ($n = 3$) and immunostaining for von Willebrand Factor (vWF) ($n = 1$) and CD68 ($n = 3$). All resected tissues with graft were fixed with 10% formalin, dehydrated with gradient alcohol and embedded in paraffin. All nerves were sectioned at 4 μm thickness and the middle parts of the grafts were used for staining. For the primary antibody, anti-vWF antibody (Dako) and anti-CD68 antibody (AbD Serotec) were used, and horseradish peroxidase-conjugated secondary antibody (Dako), 3,3-diaminobenzidine substrate (Dako) and eosin solution (Wako) were used to visualize the cells.

The total numbers of infiltrated cells and macrophages in implants and the number of blood vessels with a luminal structure were calculated. The total numbers of cells and macrophages were analyzed using free imaging soft, ImageJ (NIH). Pictures were taken at 40× magnification, and the numbers of nuclei and stained cells were counted using particle analysis tools included in the software package. In HE staining and immunostaining for CD68, three areas were randomly selected within implanted nerves. Blood vessels with a circular form with vWF positive cells inside the grafts were counted visually.

2.3. *Implantation of Graft in the Sciatic Nerve Defect*

The allogeneic acellular nerves prepared by CIP treatment were transplanted to rat sciatic nerve defect models. The recipient animals, 6 SD rats, were anesthetized by isoflurane, and both sides of the sciatic nerves were exposed. A 10-mm length of the right-side sciatic nerve was excised, and an acellular nerve graft of the same length was sutured at both stumps of the recipient nerve using 10-0 vicryl (Ethicon) under a microscope. Another side sciatic nerve was excised, and the excised nerve was reversed and sutured in the same way as the autograft control. Four of the transplanted animals underwent electrophysiological and histological study, and the others were only used for histological evaluation.

2.4. Assessment of the Transplanted Nerves

The transplanted grafts were electrophysiologically evaluated by electromyograms in the short-term (158 days; $n = 1$) and long-term (247, 248 and 258 days; $n = 1$ each) experiments. Under anesthesia, both sides of the sciatic nerves were exposed from the proximal to the distal parts of the graft positions. The proximal part of the nerve was hooked with two platinum wire electrodes and stimulated with 1 V monophagic rectangular voltage with 10 μs duration at a frequency of 1 Hz (Nihon Koden). The myogenic potential of the tibial muscle group was recorded by inserting two needle-type electrodes, amplified (Nihon Koden) and acquired by a PowerLab system (AD Instruments). In all cases, 50 traces were recorded and averaged.

In the histological evaluation, sciatic nerves including the graft were resected at 110 days ($n = 1$) and 158 days ($n = 1$) post-operation. The nerves were fixed with 10% neutralized formalin, dehydrated and embedded in paraffin. Then, the tissues were sliced longitudinally in sections of 4 μm thickness each, and the middle parts of the grafts were stained using HE or anti-glial fibrillary acidic protein (GFAP) antibody (Dako), which stains Schwann cells in peripheral nerves. The anti-GFAP was visualized with labeled polymer (Dako) according to the manufacturer's specifications. Hematoxylin staining (Wako) was carried out as a counterstaining measure to visualize the nuclei.

2.5. Statistical Analysis

The total number of cells and macrophages in the subcutaneous implantation experiments was counted. The mean values of all parameters were determined along with their standard deviations. Student's t-tests were applied to determine the statistical significance of differences between numbers of total cells and macrophages in allogeneic fresh or allogeneic acellular grafts. Values of $P < 0.05$ were considered to indicate statistical significance.

3. Results

3.1. Decellularization of Rat Sciatic Nerves

Acellular rat sciatic nerves were prepared by destroying cells using CIP treatment and a washing process. At two time points, i.e., immediately after CIP treatment or after CIP treatment plus 3 weeks of washing, nerves were histologically compared with untreated fresh nerves by hematoxylin and eosin (HE) staining and immunostaining for GFAP (Figs 1 and 2). The results showed that CIP treatment alone could not remove the cells (Fig. 1B). After the washing process, all cells were removed from the tissue, and fiber-like extracellular matrices (ECM) were left behind (Fig. 1C). On the other hand, there were many nuclei present among the dense matrices in the untreated fresh nerves (Fig. 1A). Immunostaining showed that the Schwann cells in the nerves completely disappeared after decellularization (Fig. 2B). These histological observations showed that the decellularization process

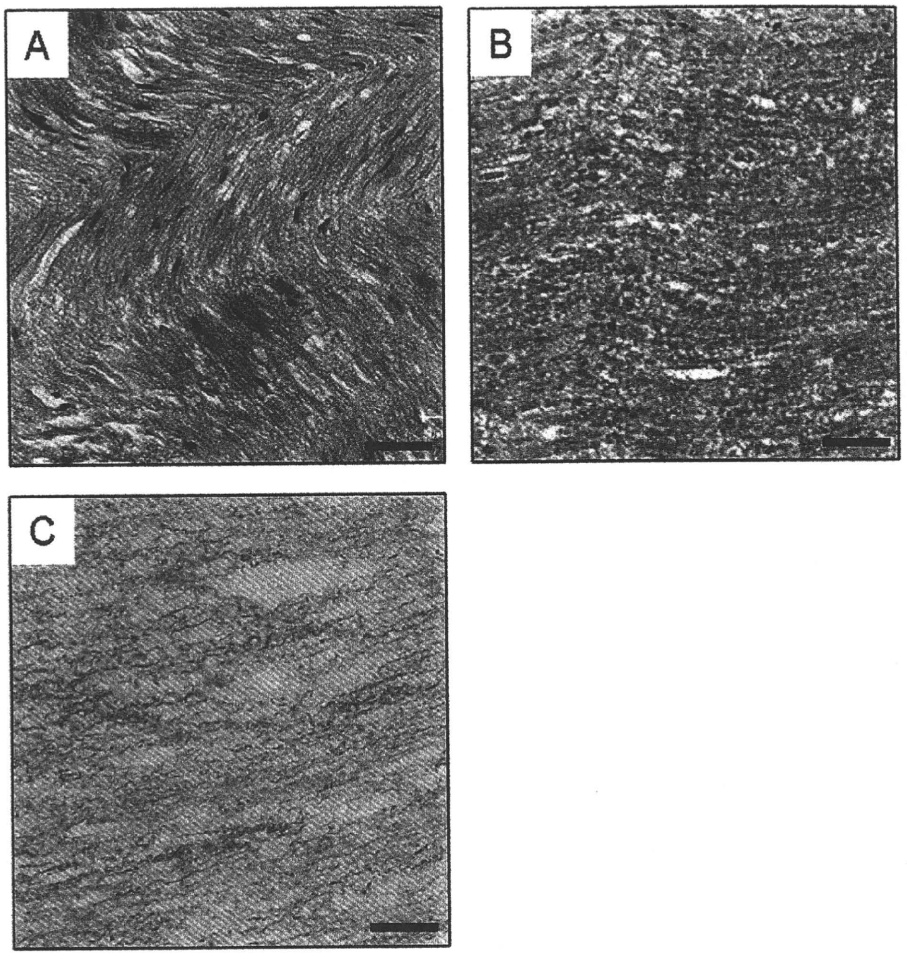

Figure 1. HE staining of a fresh nerve (A), a nerve just after CIP treatment (B) and a nerve after the complete washing process (C). Scale bars = 50 μm.

succeeded in the removal of cellular components while retaining the nerve ECM. The remaining ECM maintained an intrinsic orientation that is expected to be effective for axonal growth.

3.2. Host Body Reactions to Allogeneic Fresh and Acellular Nerves

To investigate how the decellularization process affects the host body reaction, fresh and acellular nerves of Lewis rats were implanted subcutaneously into the SD rats and assessed histologically. At 1 month post-operation, many cells had infiltrated in both grafts (Fig. 3). However, the cell shapes were quite different between the fresh nerve and the acellular nerve. Many cells in the fresh nerve showed spindle-shaped nuclei and cytoplasms, whereas round shapes were seen in the acellular nerve (Fig. 3A and 3B). Immunostaining for CD68 showed that most cells in the

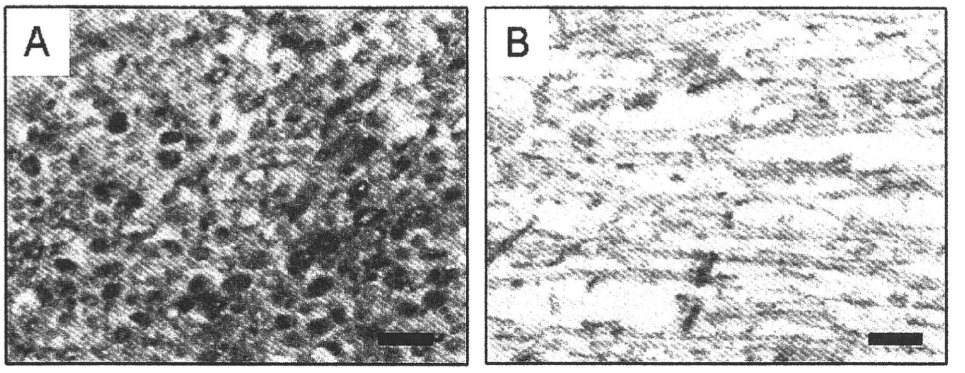

Figure 2. Immunostaining for GFAP of fresh (A) and acellular (B) nerves before implantation. Scale bars = 50 μm.

acellular nerves were macrophages while there were very few CD68-positive cells in the fresh nerves (Fig. 3C and 3D). The total numbers of cells and CD68-positive cells are summarized in Fig. 4. The total cell densities in the fresh and acellular nerves were the same. However, most cells in the acellular nerves were CD68-positive cells, whereas there were almost no CD68-positive cells in the fresh nerves. The major cell population in the fresh nerves could not be identified from immunostaining.

Angiogenesis in the graft was visualized by vWF immunostaining (Fig. 3E and 3F). When the fresh nerve was implanted, many small capillaries were present inside the graft (495 capillaries), and the surrounding subcutaneous tissue had normal vessels. On the other hand, when the acellular nerve was implanted, angiogenesis did not occur in the graft (19 capillaries), but blood vessels with a larger diameter did appear in the surrounding tissues. These observations suggest that the decellularization process might have changed the characteristics of the nerves and caused a different host body reaction in comparison to that elicited by the fresh nerves.

3.3. Histological Evaluation of the Acellular Nerve Grafts

Histological evaluation of the transplanted grafts was carried out by HE staining and immunostaining for GFAP on 110 days and 158 days after the operation (Fig. 5). Both in the fresh autograft and in the acellular allogeneic graft, remarkable cellular infiltration was observed by HE staining, even at 110 days after transplantation. Most of these cells were aligned in the longitudinal direction of the nerves, but rarely formed a fiber-like morphology at that point on time. On the other hand, 158 days after transplantation, many fibrous structures in the long-term transplantation were observed, especially in the autologous fresh nerve.

Immunostaining for GFAP in the Schwann cells in the peripheral nerves showed that the Schwann cells had infiltrated the host nerves. At 110 days post-operation,

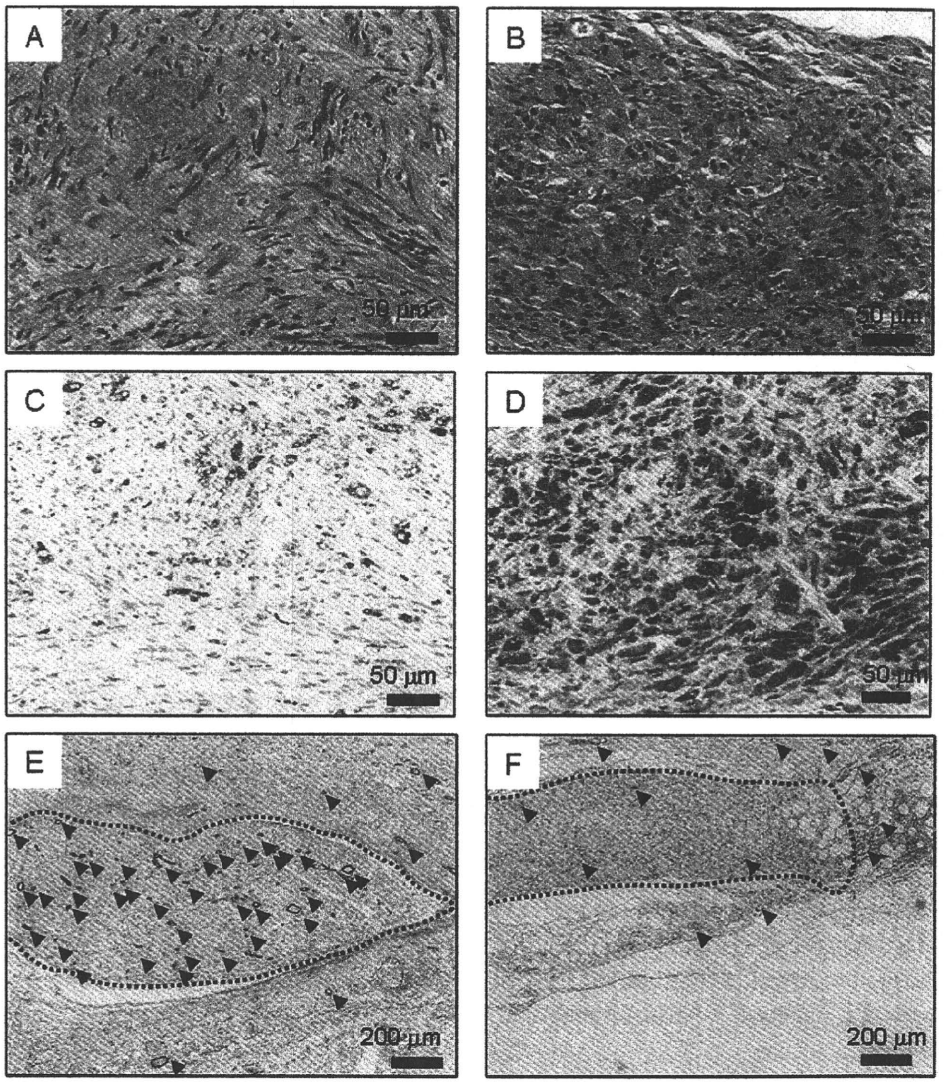

Figure 3. HE staining (A, B) and immunostaining for CD68 (C, D) and vWF (E, F) in subcutaneously implanted allogeneic fresh (A, C, E) and allogeneic acellular (B, D, F) nerves 1 month postimplantation. The images of HE staining and immunostaining for CD68 show the middle areas of the implant. The dotted lines and arrowheads in E and F indicate the edge of the grafts and microvessels, respectively. This figure is published in colour in the online edition of this journal, that can be accessed *via* http://www.brill.nl/jbs

a few GFAP-positive cells with fiber-like morphologies were observed in autologous fresh nerves but not in the allogeneic acellular graft. At 158 days after the time of transplantation, both grafts showed a fiber-like formation of GFAP-positive cells. At that time point, the acellular grafts included cells with thinner fiber-like morphology than the fresh nerves.

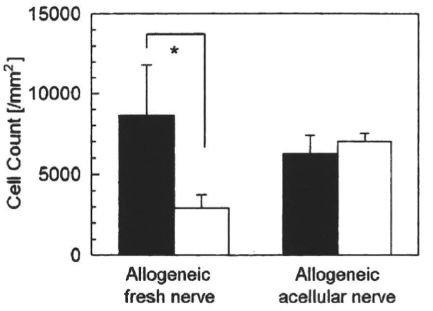

Figure 4. Number of total infiltrated cells (black column) and macrophages (white column) in the allogeneic fresh and allogeneic acellular nerves at 1-month postoperation ($n = 3$ each). Three magnified pictures were taken in each graft and the cells were counted. All data are indicated as the mean ± SD. *CD68-positive cells *vs* total cells in the fresh nerve $P > 0.05$.

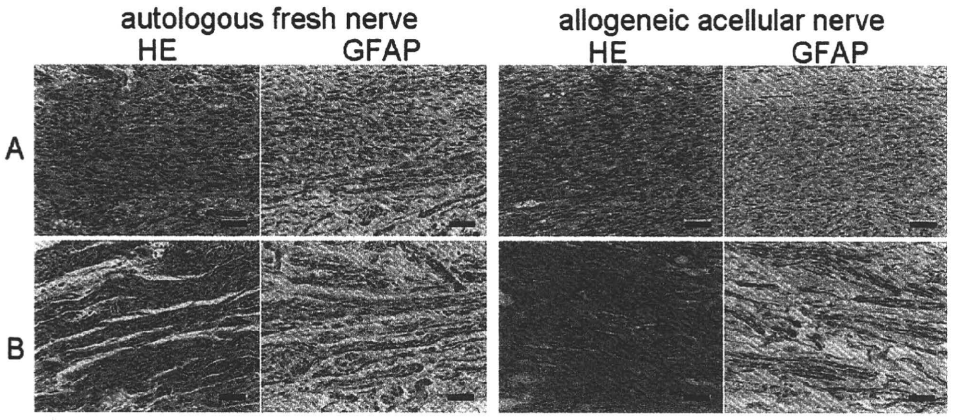

Figure 5. HE staining and immunostaining for GFAP of transplanted autologous fresh nerve and allogeneic acellular nerve (A) 110 days and (B) 158 days after operation. Scale bars = 50 μm. This figure is published in colour in the online edition of this journal, that can be accessed *via* http://www.brill.nl/jbs

3.4. Electrophysiology

Electrophysiological recovery of the allogeneic acellular nerves and autologous fresh nerves was assessed by measuring the myogenic potential of the tibial muscle group. The results from all animals subjected to the electrophysiological study are shown in Fig. 6. In the case of the autologous fresh nerves, an electrophysiological response at the tibial muscles was observed after short-term transplantation, but no reaction was seen in the acellular nerve grafts. After long-term transplantation, the electrophysiological responses in the allogeneic acellular nerve group were dramatically recovered; that is, 2 of the 3 cases showed normal reactions to the sciatic nerve stimulus (Fig. 6C). In the autologous fresh nerve group as well, only 2 of the 3 cases reacted normally to electrical stimulation. These results demonstrate that a 10-mm gap in the rat sciatic nerves can be bridged using CIP-treated allo-

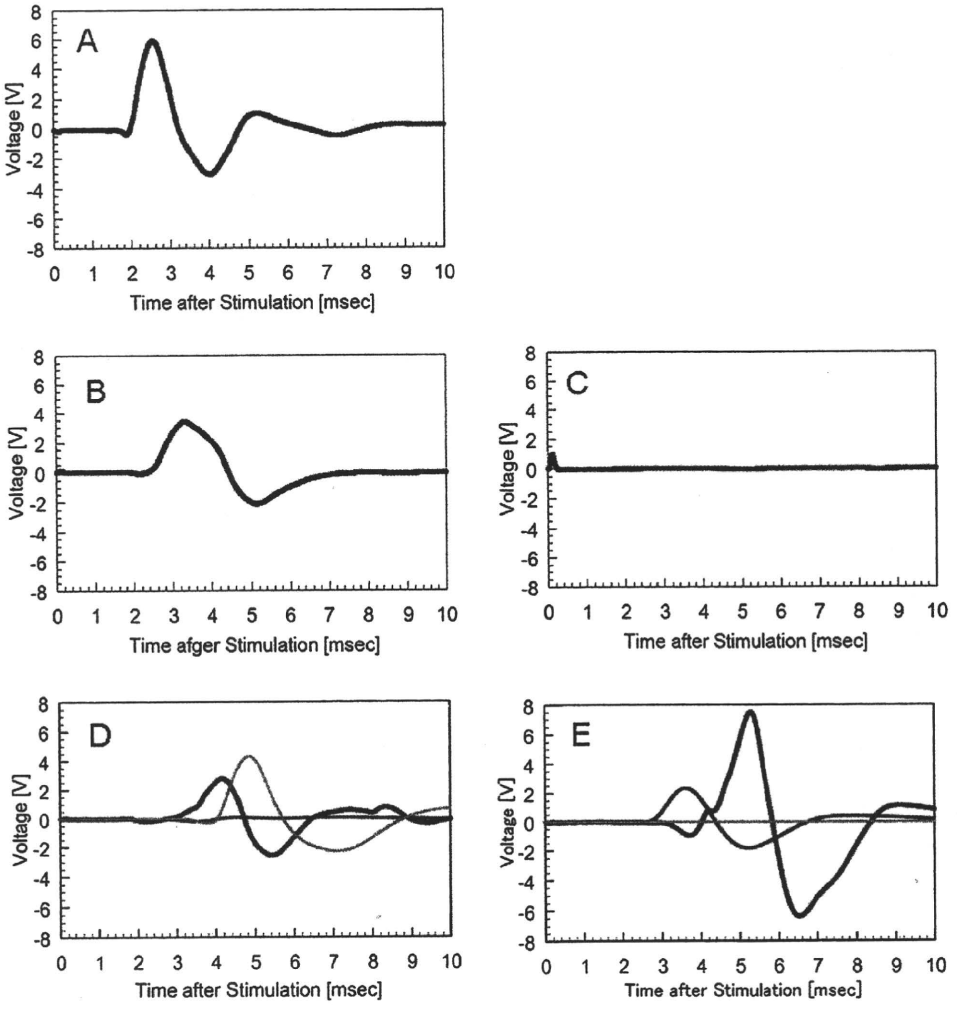

Figure 6. Averaged electromyograms of the tibial muscle of legs into which autologous fresh nerves (B, D) and allogeneic acellular nerves (C, E) were transplanted. Electromyograms before operation (A), after short-term transplantation (B, C; $n = 1$) and after long-term transplantation (D, E; $n = 3$).

geneic acellular nerves. The induced axon in that graft successfully recovered the nerve function, although the axonal growth took more time than the autologous fresh nerve did. Our results show that the myogenic potential that had completely disappeared immediately after graft transplantation was recovered thereafter.

4. Discussion

To overcome the donor shortage for peripheral nerve treatments, allogeneic acellular nerves will likely be the most viable graft for growing axons. However,

there have been only a few studies that used allogeneic animal models. In some cases, inadequate transplantation models in dogs or rats were defined as allogeneic systems [31, 33]. Rats are thought to be the best animals for investigating allogeneic transplantation because of their well-defined histocompatibility and disparity.

CIP treatment can only disrupt the cells. From this point of view, the thermal pretreatment of nerves, which is commonly used to reduce their immunogenicity, can provide the same results as our CIP treatment. However, by combining the CIP treatment with a washing process, all cells were effectively removed from the tissue. The chemical process which is commonly employed to decellularize tissue involves detergent, and that affects axonal growth. However, our washing solution did not have any such harmful component.

Electrophysiological recovery in the acellular grafts was not demonstrated in the short-term (about 5 months post-operation). It is believed that this delay of physiological recovery was caused by immature Schwann cell alignments. Although the Schwann cell alignments were observed in the acellular nerve graft 5 months after the transplantation just as in the autograft, the cells in the acellular nerve were smaller and less mature than those in the autograft. In general, from the first day to the first week following the peripheral nerve injury, macrophages are recruited in significant numbers to degenerate the axons and to remove the myelin debris for nerve regeneration. After that, the Schwann cells usually align to form pathways for the growth of axons from the proximal to distal stump of the nerve defect [34]. Thus, we evaluated the host reaction to the transplanted acellular nerves 4 weeks after implantation, since the normal reaction to injured host nerves is considered to be complete at this time point. Four weeks after the subcutaneous implantation of fresh nerves, many host cells but very few macrophages were observed in the fresh nerves (Fig. 3A and 3C), suggesting that all allogeneic cells in the transplanted nerves were removed within 1 month and replaced with the host cells. In contrast, the acellular nerves were filled with macrophages even though they did not contain any allogeneic cells when transplanted. This macrophage infiltration did not result from the incomplete removal of allogeneic cells but might have resulted from the alteration of extracellular matrix protein by CIP treatment. In fact, when the fresh and acellular nerves of SD rats were implanted in SD rats subcutaneously (isogenic transplantation), the same host reactions as in the case of the allogeneic model occurred (data not shown). It has been reported that treatment of bacteriochlorophyll with a high pressure of 0.6 GPa changed the 800-nm absorbance, reflecting a tertiary structure alteration of the protein [35]. Thus, the 980 MPa pressure used in our CIP treatment might affect the extracellular matrix structure of both allogeneic and isogenic nerves, causing them to have a much stronger foreign body reaction than that in the fresh nerve implantation. Such a large effect of CIP treatment on the ECM protein was not observed in the case of decellularization of blood vessels or cardiac valves. ECM of nerve tissue is considered to be less stable against high pressure than the fibrillar ECM of blood vessels due to the large amount of

proteoglycans. Therefore, although the acellular vessels or cardiac valves prepared by CIP treatment succeeded in tissue regeneration in animal experiments, further optimization of the CIP conditions will be needed for the nerve regeneration.

Angiogenesis is one of the inflammatory responses in material implantation. In the subcutaneous implantation study, only a low level of angiogenesis was observed in the allogeneic acellular nerves, even though many macrophages were present (Fig. 3D and 3F). On the other hand, many small vessels were observed in the allogeneic fresh nerves (Fig. 3E). We considered that the allogeneic cells were removed and host fibroblasts migrated to form granulation tissue, and then the new blood vessels were induced to provide nutritional support for these cells. In fact, different cell morphologies were observed in each of the implanted nerves (Fig. 3A and 3B). The HE staining of the allogeneic fresh nerves showed fibroblast-like cell infiltration and scar-like collagenous tissue formation in the implanted nerves, which was not observed in the acellular nerve. From these results, our acellular nerves will be suitable for nerve regeneration, even though their axonal growth was slower than that in autologous fresh nerves.

The topographical cues of nerve conduit are another important factor to be considered. A number of studies have described that the interactions between a 3-D extracellular microenvironment and axons influence neuronal growth [36]. A suitable pore size of the nerve conduits facilitates nerve regeneration. One report has shown that a macroporous synthetic nerve conduit made from poly(ε-caprolactone) with pore sizes of 1–10 μm was most effective in nerve regeneration among the bigger and smaller pore size conduits [37]. From the SEM observations, our acellular nerve had about 10 μm spaces among the remaining fibers, but failed to recover myogeneic potential even at 5 months post-operation. On the other hand, the detergent-treated allogeneic acellular nerves implanted in the 10-mm gap of a rat sciatic nerve succeeded in promoting axonal growth to the distal portion and showed good motor function, measured as electromyographic activity, within one month after the operation [20]. These good results might have arisen from the fact that their detergent-treated acellular nerves contained larger pores (20–100 μm) than our acellular nerves did. In a series of *in vitro* experiments using PC12 cells on various microchannels, Mahoney *et al.* showed that the effective widths in the neurite direction along the axis of the grooves were 20–30 μm [38]. There is expected to be a slight difference in either synthetic or tissue-derived materials between *in vivo* and *in vitro* studies. The filament diameter in the acellular nerves also affects the axonal growth activity. The optimal polypropylene filament diameter for alignment of dorsal root ganglion (DRG) neurites and outgrowth of Schwann cells has been reported to be 5 μm [39]. The combination of biomolecules with acellular nerves is expected to be another way to accelerate axonal growth. Rat acellular nerve allografts loaded with vascular endothelial growth factor and beta-nerve growth factor are reported to lead to greater axonal density at the distal portion of the graft [20].

5. Conclusion

Our allogeneic acellular nerves show promise for use as axonal scaffolds in peripheral nerve defects. As compared to allogeneic fresh nerves, the allogeneic acellular nerves did not induce scar formation in the graft, and led to a successful recovery of sciatic nerve function. Further optimization of the CIP treatment will result in fewer protein structural changes and an improvement of the spaces among the fibrous components, which may improve the regeneration rate and axon density.

Acknowledgements

This work was financially supported by a Grant-in-Aid for Young Scientists (B), a Grant-in-Aid for Scientific Research from the Ministry of Health, Labour and Welfare of Japan, and a CREST-JST grant.

References

1. J. R. Hess, M. J. Brenner, I. K. Fox, C. M. Nichols, T. M. Myckatyn, D. A. Hunter, S. R. Rickman and S. E. Mackinnon, *Plast. Reconstr. Surg.* **119**, 246 (2007).
2. D. Neubauer, J. B. Graham and D. Muir, *Exp. Neurol.* **207**, 163 (2007).
3. A. K. Gulati, *J. Neurosurg.* **68**, 117 (1988).
4. S. M. Hall, *Neuropathol. Appl. Neurobiol.* **12**, 401 (1986).
5. C. Ide, K. Tohyama, E. Yokota, T. Nitatori and S. Onodera, *Brain Res.* **288**, 61 (1983).
6. S. E. Mackinnon, V. B. Doolabh, C. B. Novak and E. P. Trulock, *Plast. Reconstr. Surg.* **107**, 1419 (2001).
7. M. Sondell, G. Lundborg and M. Kanje, *Brain Res.* **795**, 44 (1998).
8. T. W. Hudson, S. Zawko, C. Deister, S. Lundy, C. Y. Hu, K. Lee and C. E. Schmidt, *Tissue Eng.* **10**, 1641 (2004).
9. B. Hontanilla, C. Audá, J. Aucocha and O. Gorría, *Neurosurgery* **58**, 768 (2006).
10. C. B. Jenq and R. E. Coggeshall, *Brain Res.* **361**, 233 (1985).
11. T. M. Myckatyn and S. E. Mackinnon, *Neurol. Res.* **26**, 124 (2004).
12. T. Osawa, C. Ide and K. Tohyama, *Arch. Histol. Jpn* **50**, 193 (1987).
13. P. J. Evans, R. Midha and S. E. Mackinnson, *Prog. Neurobiol.* **43**, 187 (1994).
14. Z. Li, J. Peng, G. Wang, Q. Yang, H. Yu, Q. Guo, A. Wang, B. Zhao and S. Lu, *Exp. Neurol.* **214**, 47 (2008).
15. A. K. Gulati and G. P. Cole, *J. Neurosurg.* **72**, 114 (1990).
16. N. Danielsen, J. M. Kerns, B. Holmquist, Q. Zhao, G. Lundborg and M. Kanje, *Brain Res.* **681**, 105 (1995).
17. T. W. Hudson, S. Y. Liu and C. E. Schmidt, *Tissue Eng.* **10**, 1346 (2004).
18. T. Osawa, K. Tohyama and C. Ide, *J. Neurocytol.* **19**, 833 (1990).
19. J. Sørensen, K. Fugleholm, M. Moldovan, H. Schmalbruch and C. Krarup, *Brain Res.* **903**, 185 (2001).
20. B. S. Kim, J. J. Yoo and A. Atala, *J. Biomed. Mater. Res. A* **68**, 201 (2004).
21. J. M. Rovak, D. K. Bishop, L. K. Boxer, S. C. Wood, A. K. Mungara and P. S. Cederna, *J. Reconstr. Microsurg.* **21**, 207 (2005).
22. H. C. Ott, T. S. Matthiesen, S. K. Goh, L. D. Black, S. M. Kren, T. I. Netoff and D. A. Taylor, *Nature Med.* **14**, 213 (2008).

23. S. R. Meyer, J. Nagendran, L. S. Desai, G. R. Rayat, T. A. Churchill, C. C. Anderson, R. V. Rajotte, J. R. Lakey and D. B. Ross, *J. Thorac. Cardiovasc. Surg.* **130**, 469 (2005).
24. S. Mirsadraee, H. E. Wilcox, K. G. Watterson, J. N. Kearney, J. Hunt, J. Fisher and E. Ingham, *J. Surg. Res.* **143**, 407 (2007).
25. C. Ide, T. Osawa and K. Tohyama, *Prog. Neurobiol.* **34**, 1 (1990).
26. S. E. Mackinnon, A. R. Hudson, R. E. Falk, D. Kline and D. Hunter, *Neurosurgery* **15**, 690 (1984).
27. E. L. Whitlock, S. H. Tuffaha, J. P. Luciano, Y. Yan, D. A. Hunter, C. K. Magill, A. M. Moore, A. Y. Tong, S. E. Mackinnon and G. H. Borschel, *Muscle Nerve* **39**, 787 (2009).
28. T. Fujisato, K. Minatoya, S. Yamazaki, Y. Meng, K. Niwaya, A. Kishida, T. Nakatani and S. Kitamura, in: *Cardiovascular Regeneration Therapies Using Tissue Engineering Approaches*, H. Mori and H. Matsuda (Eds), p. 83. Springer, Tokyo (2005).
29. S. Hall, *J. Anat.* **190**, 57 (1997).
30. G. Keilhoff, F. Prätsch, G. Wolf and H. Fansa, *Tissue Eng.* **11**, 1004 (2005).
31. C. Ide, K. Tohyama, K. Tajima, K. Endoh, K. Sano, M. Tamura, A. Mizoguchi, M. Kitada, T. Morihara and M. Shirasu, *Exp. Neurol.* **154**, 99 (1998).
32. P. J. Evans, S. E. Mackinnon, R. Midha, J. A. Wade, D. A. Hunter, Y. Nakao and G. M. T. Hare, *Microsurgery* **19**, 115 (1999).
33. M. Nakamura, N. Tomizawa, K. Tohyama and S. Hara, *J. Vet. Med. Sci.* **66**, 767 (2004).
34. V. H. Perry, M. C. Brown and S. Gordon, *J. Exp. Med.* **165**, 1218 (1987).
35. A. Gall, A. Ellervee, J. N. Sturgis, N. J. Fraser, R. J. Cogdell, A. Freiberg and B. Robert, *Biochemistry* **42**, 13019 (2003).
36. G. N. Li and D. Hoffman-Kim, *Tissue Eng.* **14**, 33 (2008).
37. C. L. A. M. Vleggeert-Lankanp, G. C. W. de Ruiter, J. F. C. Wolfs, A. P. Pêgo, R. J. van den Berg, H. K. P. Feirabend, M. J. A. Malessy and E. A. J. F. Lakke, *J. Biomed. Mater. Res. A* **80**, 965 (2007).
38. M. J. Mahoney, R. R. Chen, J. Tan and W. M. Saltzman, *Biomaterials* **26**, 771 (2005).
39. X. Wen and P. A. Tresco, *J. Biomed. Mater. Res. A* **76**, 626 (2006).

CONTRAST MEDIA & MOLECULAR IMAGING

Received: 11 August 2009, Revised: 1 April 2010, Accepted: 8 April 2010, Published online in Wiley Online Library: 27 May 2010

(wileyonlinelibrary.com) DOI:10.1002/cmmi.389

Design and characterization of a polymeric MRI contrast agent based on PVA for *in vivo* living-cell tracking

Yoichi Tachibana[a], Jun-ichiro Enmi[b], Atsushi Mahara[a], Hidehiro Iida[b] and Tetsuji Yamaoka[a]*

A novel water-soluble MRI contrast agent for *in vivo* living cell tracking was developed. Unlike the conventional *in vivo* cell tracking system based on superparamagnetic iron oxide beads, the newly developed contrast agent is eliminated from the body when the contrast agent exits the cells upon cell death, which makes living cell tracking possible. The contrast agent is composed of gadolinium chelates (Gd–DOTA) and a water-soluble carrier, poly(vinyl alcohol) (PVA), which is known to interact with cells and tissues very weakly. Since the Gd–PVA was not taken up by cells spontaneously, the electroporation method was used for cell labeling. The delivered Gd–PVA was localized only in the cytosolic compartment of growing cells with low cytotoxicity and did not leak out of the living cells for long periods of time. This stability may be due to the weak cell-membrane affinity of Gd–PVA, and did not affect cell proliferation at all. After cell labeling, signal enhancement of cells was observed *in vitro* and *in vivo*. These results indicate that Gd–PVA can visualize only the living cells *in vivo* for a long period of time, even in areas deep within large animal bodies. Copyright © 2010 John Wiley & Sons, Ltd.

Keywords: MRI; cell tracking; intracellular delivery; cell transplantation; Gd chelate

1. INTRODUCTION

Over the past decade, there has been increasing interest in developing cell transplantation therapy (1–3) for various diseases such as ischemic limbs (4), infarcted myocardium (5,6) and diabetic retinopathy (7). In particular, the transplantation of autologous cells such as bone marrow- or fat tissue-derived mesenchymal stem cells is much safer than heterologous transplantation in terms of rejection, and is promising in clinical use. However, the mechanism of cell transplantation therapy remains a matter of debate. One possible mechanism is the differentiation of transplanted cells into functional cells, and another is the paracrine effect due to the produced cytokines (8). Moreover, even the engraftment ratio and survival period of the transplanted cells remain unclear. A general method of analyzing the transplanted cells, such as immunostaining, cannot be used for autologous cell transplantation because there is no phenotypic difference between transplanted cells and host cells. In recent years, then, noninvasive tracking systems for cell transplantation are attracting a great deal of attention (9,10).

Optical imaging methods using fluorescence- or bioluminescence-labeled cells have been studied extensively (11,12). Recently, green fluorescent protein (GFP)-transgenic animal or GFP-positive cells have become widely available and have been easily analyzed using various *in vivo* optical imaging instruments. However, since optical lights can penetrate tissues less than 10 mm in the case of fluorescence and 30 mm in the case of bioluminescence, only mice or rats can be used in this system (13). Therefore, cell transplantation model systems cannot be used for various diseases in large animals (14–16). In addition, the resolution is low, and the transplanted cells can be detected as large circles in small animals (13).

In contrast, magnetic resonance imaging (MRI) is a more promising system because of its high resolution, its absence of limitations on animal size and its noninvasiveness. In order to detect the transplanted cells in host tissues using MRI, cells should be labeled with contrast agents. In the past 15 years, superparamagnetic iron oxide particles (SPIO) have been studied as a means of labeling cells because of their high sensitivity (17,18). SPIO are superior to other contrast agents in terms of the detection of cells. Rice *et al.* reported the homing phenomena of adipose-derived stem cells in cerebral infarction (19). Stuckey *et al.* reported the monitoring of bone marrow stromal cells in the infarcted heart (20). Targeted cells were usually labeled with SPIO by the endocytosis mechanism or by using gene-transfection agents. However, in long-term tracking of cells, one of the problems with this system is the fate of SPIO which leaks out of

* *Correspondence to: T. Yamaoka, Department of Biomedical Engineering,Advanced Medical Engineering Center, National Cardiovascular Center Research Institute, Suita 565-8565, Japan.*
E-mail: yamtet@ri.ncvc.go.jp

a *Y. Tachibana, A. Mahara, T. Yamaoka*
Department of Biomedical Engineering,Advanced Medical Engineering Center, National Cardiovascular Center Research Institute, Suita 565-8565, Japan

b *J.-i. Enmi, H. Iida*
Department of Investigative Radiology,Advanced Medical Engineering Center, National Cardiovascular Center Research Institute, Suita 565-8565, Japan

Contract/grant sponsor: Ministry of Health, Labour and Welfare of Japan (Health and Labour Sciences Research Grants, Research on Nanotechnical Medical).
Contract/grant sponsor: Research Grant for Cardiovascular Diseases, Ministry of Health, Labour and Welfare of Japan; contract/grant number: 18A-2.

cells (free SPIO) due to exocytosis or cell death. Additionally, SPIO that has undergone intracellular uptake is slowly digested, releasing its iron. The free SPIO remains in the body and continues to show MR contrast, creating the potential for misunderstanding (21). Amsalem *et al.* reported that the observed MRI signals after transplantation of SPIO-labeled MSCs were not attributed to transplanted cells but to cardiac macrophages which took up the released SPIO from transplanted cells (22). Li *et al.* reported that SPIO undergoing cell death was internalized by macrophages or remained in the local tissue (23).

The most important part of cell tracking is to track only the living cells. In the present study, a novel water-soluble contrast agent was designed and an effective intracellular delivery system was established. Gd–DOTA (1,4,7,10-tetraazacyclo-dodecane-*N,N',N'',N'''*- tetraacetic acid) was conjugated to a bioinert and highly water-soluble polymeric carrier, poly(vinyl alcohol) (PVA). PVA is known to circulate for a long period of time in the blood stream *in vivo* because of its very weak interaction with the blood cells, macrophages or tissues. It was reported that the amount of PVA ingested by macrophages was much less than that of bovine serum albumin (24). The conjugates would be expected to be eliminated from the tissues without being ingested by macrophages when they are outside of the dead cells. The intracellular delivery system of the conjugates was established using an electroporation system, and the cytotoxicity, intracellular stability, body distribution and MR-imaging ability of the contrast agent were studied *in vitro* and *in vivo*.

2. RESULTS

2.1. Synthesis of Gd–PVA (*4a–d*)

Conjugates **4a–d** were synthesized in three steps using PVA with a molecular weight of 74 800 (**1**) as shown in Scheme 1. The structure of conjugates **4a–d** was confirmed by ^{1}H-NMR spectroscopy and their characteristics are summarized in Table 1. At step 1, the introduction ratios of diamine ($m/n \times 100$ in Scheme 1) were 13.2, 7.5, 3.6 and 12.9%, respectively. At step 2, DOTA-NHS-ester was completely reacted with free NH_2 groups on **2** because the peak of 2.79 ppm had disappeared. These polymers were soluble in water and DMSO and insoluble in acetone, toluene and tetrahydrofuran. The Gd (III) content of the conjugates (**4a–d**) was analyzed by inductively coupled plasma atomic emission spectroscopy. To observe the cell labeling efficiency and the intracellular distribution of the conjugates, Gd–PVA labeled with fluorescence (**4d**) was synthesized. MR imaging of labeled cells was carried out after confirming the cell uptake of **4d** with fluorescent microscopy. By contrast, the cytotoxicity assay was performed using **4b** without FITC because the wavelength of FITC overlapped with that of the WST assay.

The increase of the relaxivities (R_1) of **4a–d** with the increased introduction ratio of DOTA may be due to an increased rotational correlation and constructive restriction of motion. A maximum reflexivity value of 7.1 $mM^{-1}s^{-1}$ was observed at 13.2 mol% (**4a**). All of the relaxivities of **4a–d** were higher than that of clinically used Gd–DTPA (5.1 $mM^{-1}s^{-1}$), suggesting that each conjugate can be used as an effective contrast agent.

2.2. *In vitro* T_1-weighted MR measurements of polymer solutions

Figure 1 shows the MR images of **4d** solutions with different concentrations at 4.7 T. The T_1-weighted MRI signal of the **4d** solution increased with the increased polymer unit concentration. Significant contrast enhancement was seen over 0.2 mM. To achieve cell imaging, it is necessary to introduce the contrast agents at sufficient concentrations in the cells.

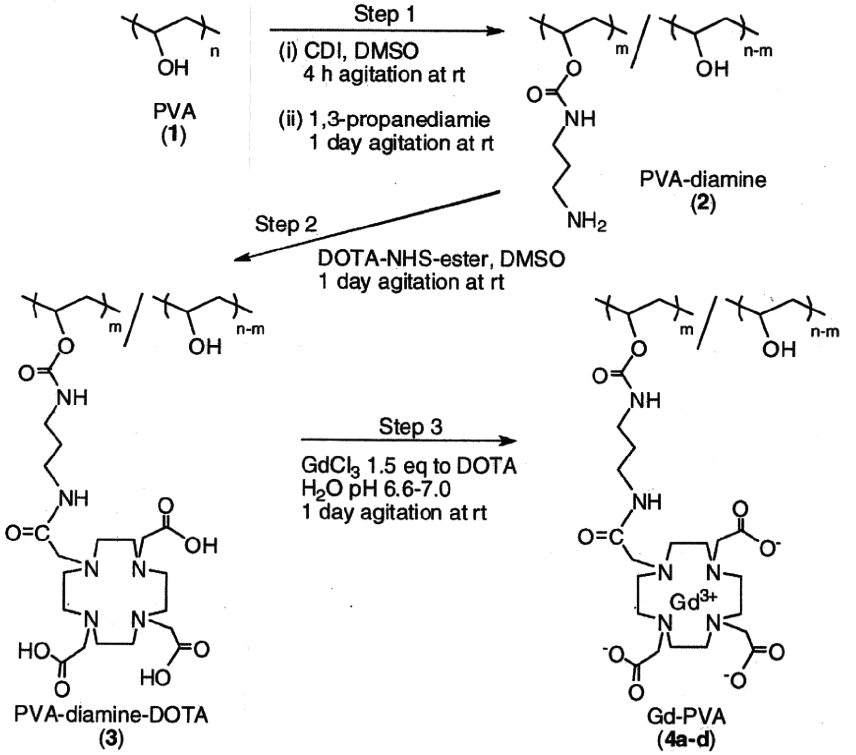

Scheme 1.